Sensors and Actuators B 250 (2017) 100–110

Contents lists available at ScienceDirect

Sensors and Actuators B: Chemical

journal homepage: www.elsevier.com/locate/snb

Characterization of a 1024 × 1024 DG-BioFET platform

Carlos Duarte-Guevara[a,f], Vikhram Swaminathan[b,f], Bobby Reddy Jr[f], Chin-Hua Wen[c], Yu-Jie Huang[c], Jui-Cheng Huang[c], Yi-Shao Liu[d], Rashid Bashir[e,f,*]

[a] Department of Electrical and Computer Engineering, University of Illinois at Urbana-Champaign, 306 N. Wright St., Urbana, IL 61801, USA
[b] Department of Mechanical Science and Engineering, University of Illinois at Urbana-Champaign, 1206 W. Green St., Urbana, 61801, IL, USA
[c] Taiwan Semiconductor Manufacturing Company, 9 Creation Rd, Hsinchu Science Park, Hsinchu, Taiwan 300-77, R.O.C. Hsinchu, Taiwan
[d] Research and Ecosystem, Delta electronics Inc., 417939, Singapore
[e] Department of Bioengineering, University of Illinois at Urbana-Champaign, 1270 Digital Computer Laboratory, 1304 W. Springfield Ave., Urbana, IL 61801, USA
[f] Micro and Nanotechnology Lab, University of Illinois at Urbana-Champaign, 208 N. Wright St., Urbana, IL 61801, USA

ARTICLE INFO

Article history:
Received 14 January 2017
Received in revised form 8 April 2017
Accepted 17 April 2017
Available online 21 April 2017

Keywords:
1024 × 1024 array
Dual-gate
Biological field-effect transistor
Beyond nernstian limit
Multiplexed biosensing
pH sensor

ABSTRACT

The use of biological field effect transistors (BioFETs) for the detection of biochemical events will yield new sensing systems that are smaller, less expensive, faster, and capable of multiplexing. Here, we present a novel massively parallel dual-gated BioFET (DG-BioFET) platform with over a million transistors in a 7 × 7 mm^2 array that has all these benefits. Utilizing on-chip integrated circuits for row and column addressing and a PXI IC tester to measure signals, the drain current of each sensor in the 1024 × 1024 array is serially acquired in just 90 s. In this paper, we demonstrate that sensors in our massively parallel platform have standard transfer characteristics, high pH-sensitivity, and robust performance. In addition, we use the dual-gate operation and fast acquisition, unique in our platform, to improve the sensing performance of the system. We show that tailored biasing of the two DG-BioFET gates results in signal amplification above the Nernst limit (to 84 mV/pH) and redundancy techniques facilitate differential referencing, improving the resulting signal-to-noise ratio. Our platform encompasses the advantages of semiconductor-based biosensors, and demonstrates the benefits of high parallelism and FET dual-gate amplification for electrical and miniaturized biological sensing.

1. Introduction

Biological field effect transistors (BioFETs) are becoming important and convenient biosensing platforms. These transistors offer simple, inexpensive, and miniaturized transduction of biomolecular reactions into potentiometric signals enabling new applications and sensor designs [1–3]. The use of BioFETs as the transduction elements offer important advantages over other biosensing methods. BioFETs can detect the intrinsic charge of analytes or reactions, and do not require preparatory labeling stages that add cost and complexity [4]. BioFETs are also CMOS compatible, enabling a seamless integration with other on-chip circuitry required for data acquisition and the large-scale manufacturing that reduce cost and size [5,6]. Finally the top-down parallel BioFET fabrication yields multiplexed detection systems allowing screening and high-throughput assays [7]. Researchers have already successfully exploited these benefits of FET biosensors in new biosensing platforms. For example, BioFETs are used in DNA sequencing platforms that exploit massive parallelism to simultaneously monitor multiple nucleotide incorporations [8,9]. Also, these transistors are the sensing element in small point-of-care biosensors that minimize footprint by avoiding the use of optical components [10,11]. Moreover, multiple studies have demonstrated that the FET geometry can be manipulated to enhance the sensitivity to surface potential changes enabling direct molecular detection and real-time identification of proteins [12,13]. BioFETs have demonstrated to be an important alternative for biomolecular applications and promise to spawn the next generation of inexpensive, small, and simple to operate biosensors.

The multiplexing ability of BioFETs has been identified previously as one of the key benefits of electrical methods but only few studies have developed platforms that use large parallelism for spatial and temporal monitoring applications. The most relevant example is the Ion Torrent sequencing chip, which uses large

* Corresponding author at: 1270 Digital Computer Laboratory, 1304 W. Springfield Ave Urbana, IL 61801, USA.
E-mail addresses: carlos@finnegan.com (C. Duarte-Guevara), rbashir@illinois.edu (R. Bashir).

http://dx.doi.org/10.1016/j.snb.2017.04.107
0925-4005/

arrays of extended gate FET sensors for DNA sequencing [8]. In Ion Torrent's chip, FET sensors are buried in inter-dielectric layers and a floating extended gate transports charge from millions of beads (where DNA amplification reactions take place) to the sensor. Other recent BioFET arrays are being employed for applications outside DNA sequencing. For instance, a 256 × 256 Ta2O5 extended-gate FET array has been recently developed to monitor hexokinase concentration [14], and the pH sensitivity of Si3N4 sensors was evaluated in a high-resolution ion camera [15]. Other recent examples include a platform of 64 BioFETs built to monitor extra membranous pH and cellular behavior by configuring FET sensors as CMOS inverters and switches [16], and 128 × 128 arrays of foundry-fabricated dual-gated BioFETs have been used for the detection of DNA binding events and urea byproducts [17]. These platforms are the basis for new approaches of high-throughput screening that leverage the high scalability of the CMOS processes to create parallel sensors that monitor multiple reactions or study the spatial and temporal behavior of biological entities [18]. Platforms with many BioFETs have demonstrated that the incorporation of electronics into biosensing applications creates new tools with promising biomolecular applications and clear advantages over traditional instruments.

In this paper, we present a new massively multiplexed dual-gated biological FET (DG-BioFET) biosensing platform with enhanced capabilities over the ones published in the past. We report a DG-BioFET array of 1024 × 1024 transistors, distributed in a 7 × 7 mm2 area, fabricated with a 0.18 μm silicon on insulator (SOI) process having a high-K hafnium oxide sensing layer and individually addressable metal-oxide-semiconductor (MOS) back-gates. While the DG-BioFET platform has standard electrical characteristics and pH sensitivity, it has unique features that enable biasing schemes to amplify the measured signal and improve the signal-to-noise ratio by facilitating differential referencing. Our platform combines a new sensor structure, with a large sensing area, and novel reading mechanisms to create a powerful sensing system that will allow users to optimize the sensors' response. In the following sections, we describe the DG-BioFET system and operation, demonstrate how the massive number of sensors in the array facilitate differential referencing, and show how the sensitivity of the sensors can be tailored in a dual-gate operation mode.

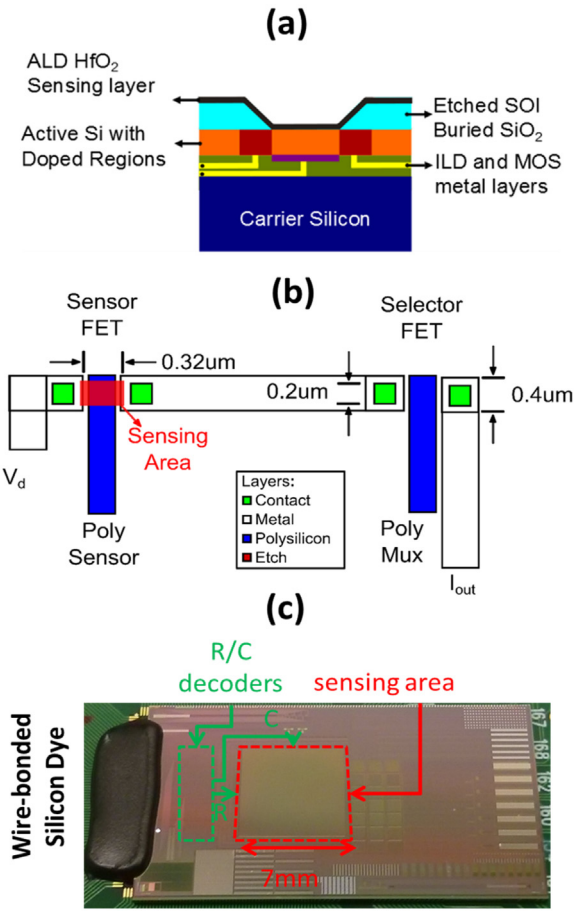

Fig. 1. DG-BioFET schematics and chip photograph. (**a**) Cross section of the sensing element in the array. (**b**) Top-view of pixel schematic in the array (**c**) Photograph or the DG BioFET array, showing the 7 × 7 mm^2 sensing area, decoding portions, and wire-bonds to PCB.

2. Fabrication and operation

2.1. Device fabrication

The array of DG-BioFETs is fabricated at Taiwan Semiconductor Manufacturing Company (TSMC) foundries without any required post processing steps. A detail step-by-step sensor fabrication flow chart was described earlier [19] and in this new array similar processes are used to manufacture the on-chip circuitry used to quickly measure the full array. Briefly, MOSFET transistors are fabricated with a standard multi-layer CMOS process on the 200 nm device layer of an SOI wafer. These initial set of transistors define the back-gate of future DG-BioFET sensors and create the logic gates that make multiplexers, decoders, and selection elements required for row and column addressing. To test the reliability of the decoding circuits, selector transistors in the diagonal across the chip are disconnected from row and column AND gates creating 'dummy' pixels within the array becoming an embedded control that test the correct addressing of sensors in the array. After the initial standard CMOS fabrication, the top of the SOI wafer is bonded to a carrier wafer, the full structure is flipped upside down, and −while still in the processing line- the SOI handling silicon is etched with chemical mechanical polish (CMP) revealing the SOI buried oxide. This oxide is carefully dry-etched in the sensor and contacts pad areas, and hafnium oxide is ALD-deposited over the entire wafer creating the DG-BioFET sensing membrane. A schematic of the resulting sensor structure is presented in Fig. 1(a). This sensor can create two inversion channels, one at the top controlled mainly by the fluid-gate, and one at the bottom controlled by the back-gate. A top-view of a simplified pixel architecture is presented in Fig. 1(b) that shows the selector transistor configuration for row and column addressing. This figure does not present all the metallization layers, control structures, biasing buses, and connecting vias. All these other not presented structures, consume significant real state in the chip and result in a larger pixel size. However, the 7 × 7 μm^2 is actually desirable for a high-density biosensor chip for a range of biological applications that use conventional microarray spotters of similar spot size for functionalization steps.

The finalized chip is mounted on a PGA 256 pin printed-circuit board (PCB) and 48 contact pads are wire-bonded to the board for electric access to the silicon die. The pads are used to supply voltage to the array, access the FET's drain/source/gate nodes, and specify the address of the selected transistor. The wire-bonds are then encapsulated with an epoxy matrix DP270 black (3 M, St. Paul, MN), a crucial step to improve robustness of connections during biosensing assays. A finalized chip is presented in Fig. 1(c), indicating the DG-BioFET array sensing area, the position of the logic transistors used for 2 dimensional row and column addressing, and the wire bonded pads.

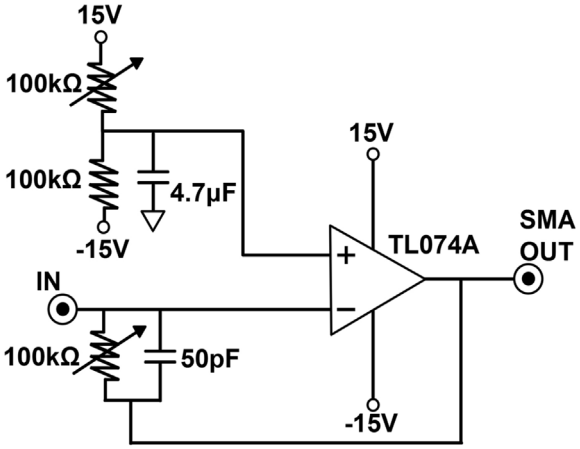

Fig. 2. Transimpedance amplifier and biasing circuit, converting I_{DS} to the input voltage for the reading card in the IC tester.

2.2. Experimental setup

For pH experiments, a 600 μL PDMS well is bonded to the chip without covering the sensing area. The chip (now mounted in the PCB) is then connected to a 256 pin socket (Integrated Service Technology, Hsinchu, TW) that establishes connections between the silicon die and a PXI logic IC tester. The tester includes trigger and reading cards, PE16A/S and PEMU32 respectively (OpenATE, Hsinchu, TW), that are synchronized with a Spectrum transient recorder (Spectrum, Grosshansdorf, DE) with all three cards housed in a NI PXI-1033 chassis (National Instruments, Austin, TX). The trigger card of the IC tester supplies voltages to the decoding circuits to select the desired transistor and set biasing conditions, while an off-chip trans-impedance amplifier (Fig. 2) routes the DG-BioFET drain current to reading circuits that records serial measurements at a rate of around 0.11 ms. The trans-impedance amplifier (TIA) settling time is below 10 μs leaving the limiting reading factor to the card switching. Therefore, the full array of 1024 × 1024 devices is measured in around 90 s. The full process is coordinated with customized MTS3 software (OpenATE) and the output is presented in the form of comma separated values files. In addition, the MTS3 software allows the user to select devices to be measured to reduce the measurements cycle. For instance, applications that are interested in capturing kinetic events and require time resolutions of less than 90 s may reduce the number of measured sensors to decrease the time length of each measurement cycle.

Equivalent systems can be built with other acquisition cards, like the Chroma 36010, virtual IC analyzers (i.e. ElVIS II from NI), or general IC testing systems like the ones offered by Keithley.

2.3. pH response characterization

Five 10 mM PBS solutions of different pH are prepared by titrating HCl and NaOH in specific concentrations. The resulting pH of these calibration solutions is measured with an Orion 3 star pH meter (Thermo Scientific, Pittsburgh, PA) and used to evaluate the DG-BioFET pH sensitivity. The solutions are manually pipetted in the PDMS well, the sensors are allowed to stabilize for 10 min, and a leak-free Ag/AgCl reference electrode (Warner Instruments, Hamden, CT) is immersed in solution to set the electrolyte potential. A picture of the full setup that includes the PDMS well, reference electrode, and PCB is presented in Fig. 3. The drain current of each transistor is obtained for a specific biasing condition creating a drain current map for a given gating voltage. The PBS solution is swapped to the next pH and potential changes induced by protonation and deprotonation of the sensing layer are observed as current changes [20].

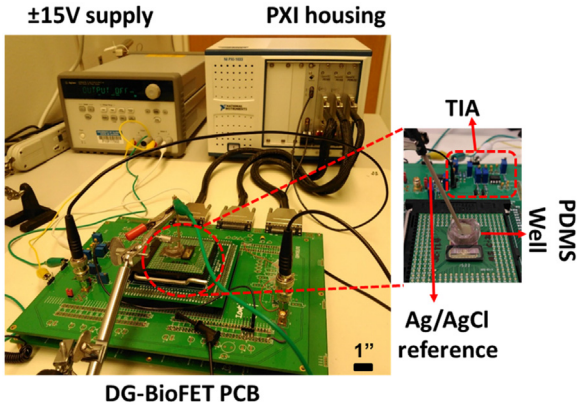

Fig. 3. Picture of the testing setup describing the PCB, PXI cards, reference electrode and PDMS well.

2.4. Data analysis

Data collected in the NI reader is compiled with Matlab scripts that average drain current measurements (each transistor is interrogated up to 15 times) and arrange data in a two-dimension matrix for each measurement. The pH sensitivity is determined by taking the derivative of the electrolyte pH vs. I_{DS} relationship both for the full DG-BioFET array and single sensors. The drain current pH sensitivity is then converted to the traditional surface potential sensitivity by multiplying current variations with the transistor's transconductance, which is obtained from transfer characteristics, using the relation (1) for the triode region [21]. Where $S_{I_{ds}}$ represents the current pH sensitivity, S_{V_g} gate voltage pH sensitivity, and g_m the device's transconductance.

$$S_{I_{ds}} = g_m * S_{V_g} \tag{1}$$

With sensitivity values, it is possible to determine the sensor's pH resolution (minimum detectable pH change) by dividing DG-BioFET noise over sensitivity (2), having the noise of the system equivalent to the standard deviation of the drain current measurement [22]. Where $pH_{\{min\}}$ represents the resolution in pH units, σ noise, and S the sensitivity.

$$pH_{\{\min\}} = \frac{\sigma}{S} \tag{2}$$

3. Electrical characterization and sensitivity analysis

3.1. Transfer characteristics

Figs. 4–6 show the transfer characteristics of transistors in the array plotting the drain current as a function of the fluid- and back-gate potentials. The transistor back-gates (BG) are swept from 0 to 1 V with a drain voltage of 2 V and 0 V in the fluid-gate (reference electrode) to obtain back-gate transfer curves. Each transistor has an individual back-gate that is set to a specific potential and the resulting current of each sensor is recorded. Fig. 4 is a 3D plot of the matrix presenting the multiple drain currents for each sensor as a result of different V_{BG} tensions. Fig. 5(a) shows a heat map that presents the top-view of Fig. 4. It shows the drain-current in the array when V_{BG} is set at 1 V and reveals the 'dummy diagonal' that is used to assure the reliability and proper status of the decoding circuits that are utilized for row and column addressing. Finally, Fig. 5(b) presents the quantification and the transfer function with error bars representing the standard deviation of all the

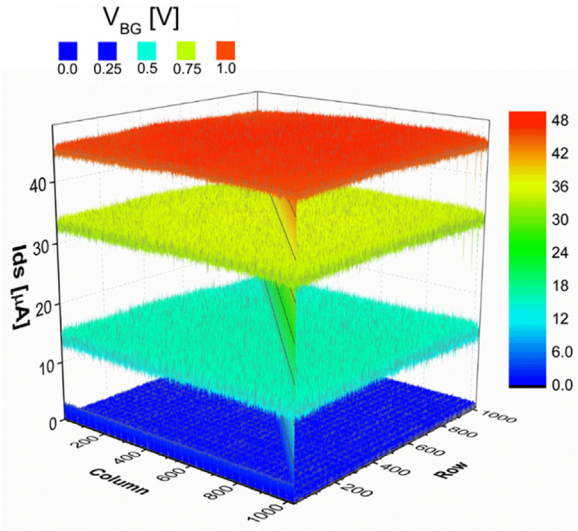

Fig. 4. 3D map of each sensor's drain current in the 1024 × 1024 array as a function of V_{BG}.

sensors in the array excluding the dummy elements in the diagonal. Results presented in Fig. 5 demonstrate standard transistor characteristics, overall back-gate transconductance (gm_{BG}) of 0.05 μA/mV in inversion, mean current standard deviations of 0.9 μA, and low variations across the chip. It also shows that the drain current seems to saturate at large voltages. This is caused by the acquisition card protection circuits that truncate values above defined threshold resulting in the apparent saturation.

Similar measurements are performed to characterize the fluid-gate (FG) using an Ag/AgCl electrode that bias a base electrolyte of pH 7.7 and all the transistors in the array. Fig. 6(a) shows the drain current heat-map when the fluid-gate is set at 2.5 V, back-gate at 0 V, and drain voltage of 2 V. The same diagonal present in the back-gate heat map exists in the fluid-gate and it's used as an embedded control of the addressing circuits. The transfer characteristic of I_{DS} as a function of the electrolyte potential (V_{FG}) is shown in Fig. 6(b) that presents a standard transfer characteristic with an overall fluid-gate transconductance (gm_{FG}) of 0.01 μA/mV in inversion and average standard deviation of 1.6 μA.

3.2. pH sensitivity

The sensitivity to pH changes of the transistors is commonly used as performance metric of BioFET sensors [4]. We evaluated the DG-BioFET array pH sensitivity by modifying the electrolyte's pH as described in the methods section. Fig. 7(a) shows the pH-dependent drain current heat maps obtained from the DG-BioFET sensors when the electrolyte is biased at a constant 2 V but the solution's pH is changed. Decrements in pH cause the protonation of the sensing membrane which result in surface potential increments that are transduced as a greater current in NMOS devices. The opposite occurs when the pH of the electrolyte increases and deprotonation events will modify the DG-BioFET's current. The overall response to pH changes is observed in the drain current quantification of Fig. 7(b) that reveals lower drain currents as the pH of the electrolyte increases. Each data point in Fig. 7(b) is the mean current measured for all devices and the error bars represent the standard deviation of all the DG-BioFET drain currents recorded in the array, excluding dummy elements, a total of 1,047,552 data points. Within the specified pH range we observed a linear response (with R^2 of 0.97) but more acid or basic electrolytes diminish the quality of the response and sensor robustness. Fig. 7(c) presents similar information but in terms of surface potential that is computed with relationship (1) and the transconductance obtained from the overall fluid-gate transfer curve (Fig. 6(b)). The results of the platform characterization experiments along with geometrical and operational array features, are summarized in Table 1, which includes other experimentally defined operational parameters such as dynamic range, power supply and consumption.

Table 1
DG-BIOFET Sensor array specifications and characteristics.

Specification	Value
Technology	0.18 μm
DG-BioFET count	1048576
Sensing Membrane	HfO_2
Sampling rate	0.11 ± 0.028 ms
Average BioFET pH sensitivity	45.8 ± 5.4 mV/pH
Average BioFET pH resolution	0.25 ± 0.09 pH
Dynamic range	4–10 pH
Center to center pitch	6.5 μm
Voltage Supply	15 V
Sensing Area	0.5 × 0.26 μm
BioFET W/L	3.8 μm/0.32 μm
Power Consumption	100 mW

The pH sensitivity analysis reveals an average response, for the entire array, of 45 mV/pH and significant variations across the drain currents recorded in the array. Hafnium oxide has been used in the past as the sensing layer for BioFETs with near Nernstian sensitivity but in our array we observe a lower response [22,23]. When inspected in detail, the drain current maps show areas that are pinned to a specific value that reduce the overall sensitivity and contribute to large deviation between devices in the array. There are 3 factors that affect the pH response in these regions. First, variations and defects in the sensing membrane prevent the expected electrochemical exchange in the dielectric resulting in lower and

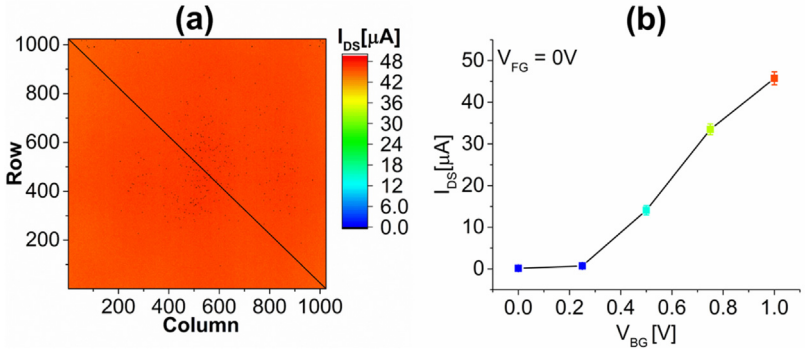

Fig. 5. Transfer characteristics of DG-BioFET back-gate. (**a**) I_{DS} heat map for a back-gate potential of 1 V. The dummy diagonal is used as an embedded control of the decoder performance. (**b**) V_{BG} Transfer characteristic of the overall population of DG-BioFETs.

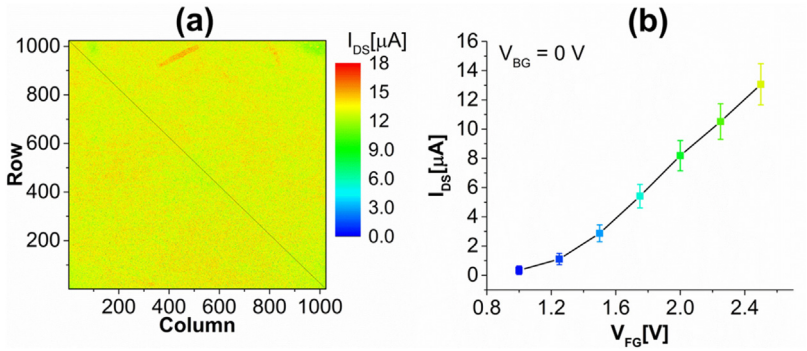

Fig. 6. Transfer characteristics of DG-BioFET fluid-gate. (**a**) I_{DS} heat map for a fluid-gate potential of 2.5 V. (**b**) V_{FG} Transfer characteristic of the overall population of DG-BioFETs.

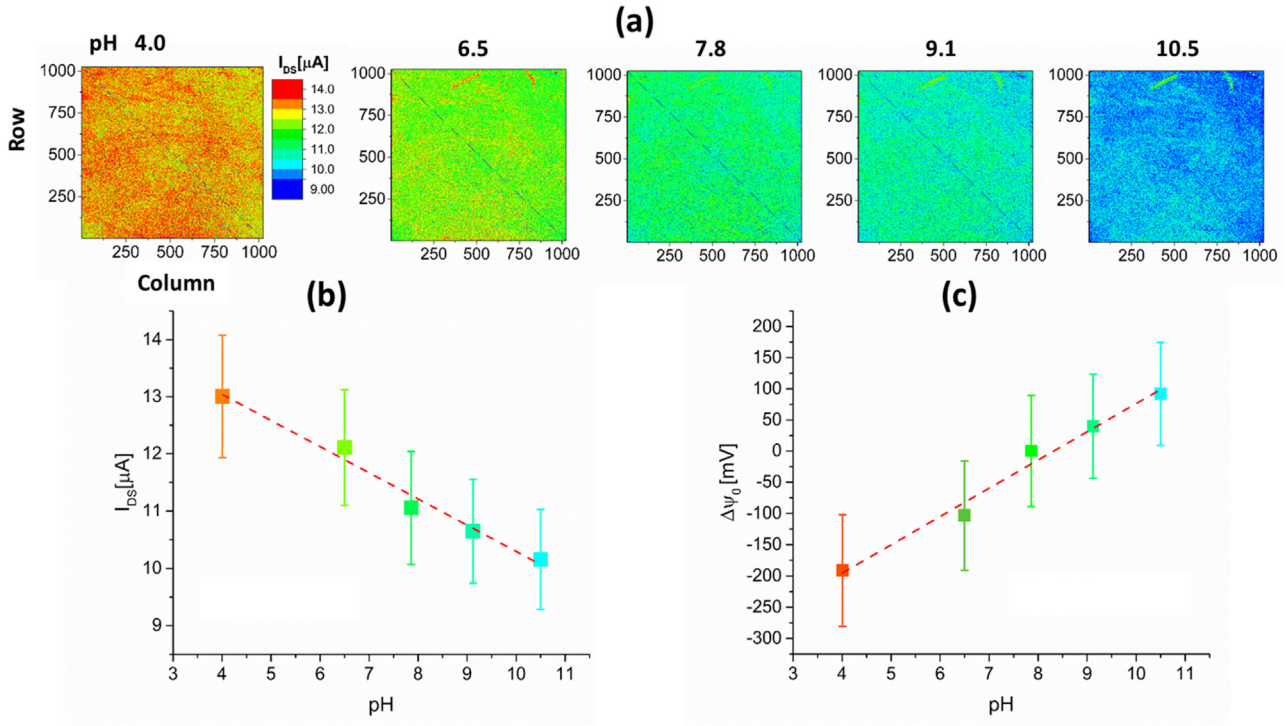

Fig. 7. DG-BioFET array pH sensitivity. (**a**) Progression of current heat-maps as a function of the electrolyte's pH. (**b**) Drain-current changes as a function of pH. (**c**) Surface potential changes as a function of pH. Error bars represent the standard deviation of all currents measured in the array.

diverse sensitives. The ALD deposition of HfO_2 in our array is an experimental process with variable chemical and physical characteristics across the array. Different chemical compositions locally modify the surface buffer capacity and thickness variations affect the oxide capacitance. Both of these dielectric variations directly influence the pH sensitivity. A second contribution to sensitivity variations comes from the selector transistors that introduce a pH insensitive current into the reading. As it is shown in Fig. 1(b), the on-chip circuitry for row and column addressing uses selector devices connected in series to choose specific drain- source nodes. Poor performance of these selector transistors (i.e. variations in threshold voltage or high device noise) will increase noise and modify applied voltages, thus affecting the sensitivity and resolution of drain current readings. Finally, in an area of $7 \times 7\,mm^2$, variations in the referencing potentials will results in lower sensitivities, increased noise, and topographical variations. Biasing changes in any of the FET nodes will modify its operation point and the recorded sensitivity. In particular, we have observed currents in the Ag/AgCl reference electrode between 0.1–0.4 nA attributed to leakage pathways through the dielectric. When in solution, even small defects in the dielectrics will result in faradaic currents between the reference electrode and the multiple nodes on the chip. These small currents in the electrolyte will cause sporadic fluid-gate fluctuations that also contribute to sensitivity variations. Therefore, defects in the sensing membrane, non-idealities in the selector circuits, and lack of uniformity in biasing conditions, explain the variations and non-ideal sensitives observed in the pH characterization. Accordingly, in our array a more accurate sensitivity assessment can be done by individually analyzing each pixel. The above-referenced topological variations can be obviated if the transconductance and response to pH changes of each sensor is recorded individually to independently calculate sensitivity and resolution. The following section presents an individual pixel analysis which also allows the study of sensitivity distributions.

3.3. Individual pixel analysis

An individual pixel pH sensitivity and resolution analysis is presented in Fig. 8. In contrast to the measurements presented for Section 3.2, which used the array transconductance to determine

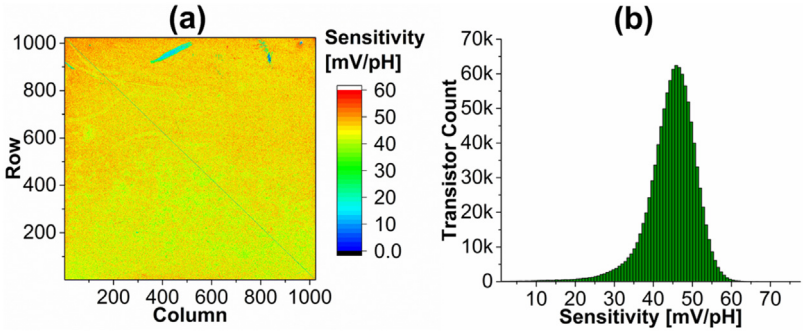

Fig. 8. Individual pixel analysis of sensitivity. (**a**) Color-coded surface potential pH sensitivity. (**b**) Distribution of DG-BioFET surface potential sensitivities in the array.

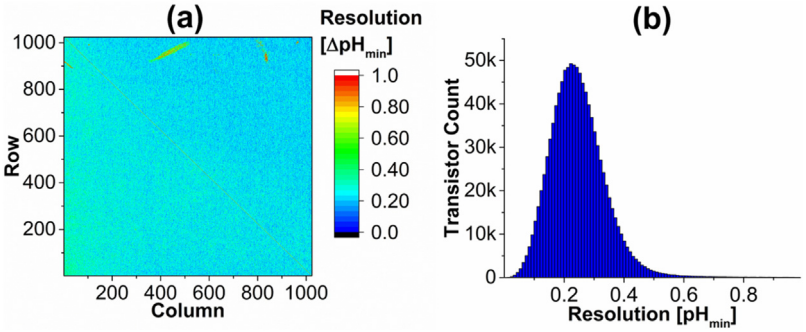

Fig. 9. Individual pixel analysis of resolution. (**a**) Color-coded pH resolution. (**b**) Distribution of pH resolution of ISFETs in the array.

an average sensitivity, in the present section the transconductance is calculated individually. Then, independent current responses are used in Eqs. (1) and (2) to estimate pH sensitivity and resolution for each device. Fig. 8(a) shows a sensitivity heat map that color-codes the surface potential response as a function of the electrolyte's pH. Each pixel in Fig. 8(a) represents the sensitivity estimated for an individual device. Fig. 8(a) clearly shows spatial sensitivity variations in the array, confirming that current variability is related with processing, circuitry, or biasing defects that locally affect the sensing performance. The distribution of sensitivities for the million different DG-BioFETs in the array is presented in Fig. 8(b). It presents a lightly negatively skewed normal distribution with a mean μ of 45.8 mV/pH and standard deviation σ of 5.4 mV/pH. Similar figures are presented in Fig. 9 that shows the heat map of each sensor's resolution (minimum detectable pH change) and the corresponding distribution. In Fig. 9(a) pixels represents the estimated resolution for each device using Eq. (2) and the individually calculated sensitivity and standard deviation. The resolution is calculated as the ratio between the DG-BioFET's noise and sensitivity. Therefore, the resulting resolution distribution is the inverse of sensitivity, a positively skewed normal distribution with a mean μ of 0.25 pH and standard deviation σ of 0.1 pH.

The ample sample size available with the DG-BioFET array reveals important aspects of the sensor behavior when analyzed as a population. The skewed characteristic of both distributions is explained by the non-idealities discussed above and the rigid upper physical limit of the Nernst equation that sets a maximum sensitivity of 59 mV/pH. The defects in the hafnium oxide membrane and readout circuitry cause variations in sensitivity, but those variations cannot overcome the intrinsic sensitivity limitations of the maximum electrochemical response. The effect of non-idealities in the platform reduce the sensitivity of devices but never increases it above the Nernst limit resulting in the skewed distributions that we observe. The positively skewed resolution distribution is also explained by the upper Nernst sensitivity limit. The relationship between sensitivity and resolution (2) and a low correlation between sensitivity and noise, result in the tail to higher resolution values of Fig. 9(b).

3.4. DG-BioFET sensors drift and noise spectrum

BioFETs are known to be subject to changes due to temperature effects, hysteresis, and drift [5]. Different techniques have been studied to correct these events and improve the stability of the sensors [24]. However, the reduction of these undermining effects by optimizing quality of manufacturing steps and materials is an alternative that has demonstrated success in the past [25]. The DG-BioFET sensing array has been carefully studied and developed to optimize measurements stability. Even though spatial variations are observed in different devices, the performance of these foundry-fabricated sensors is highly robust. Fig. 10 presents a drift analysis of the DG-BioFET array by sampling drain current

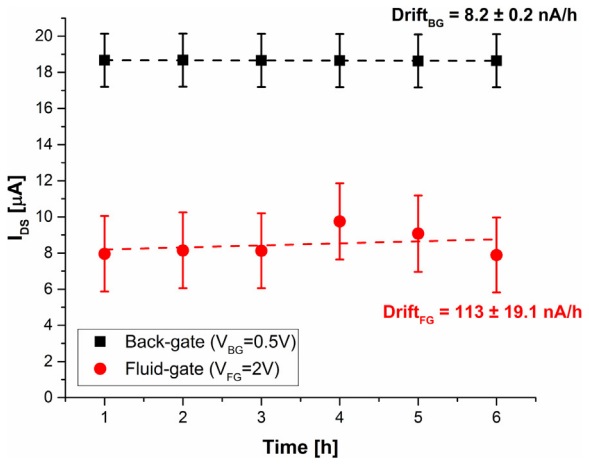

Fig. 10. Drift analysis for the fluid and back gates.

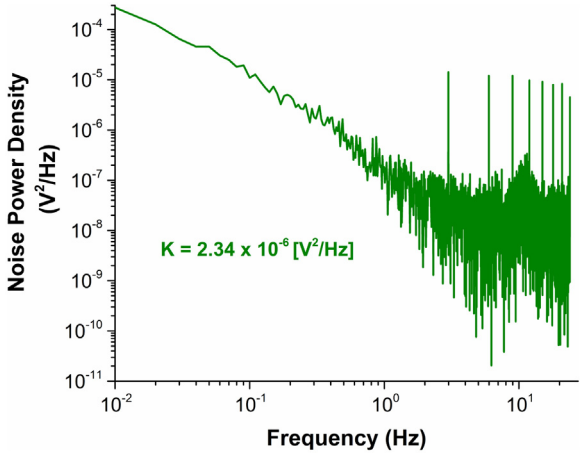

Fig. 11. Noise spectrum analysis and flicker coefficient.

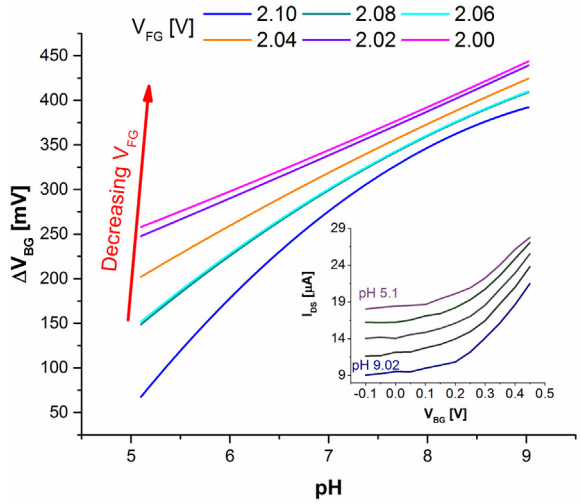

Fig. 12. Back-gate potential changes in the dual-gate operation as a function of pH for multiple biasing conditions. The inset presents back-gate sweeps as a function of pH.

at constant biasing conditions for every hour during a 6-h period. The results demonstrate that both the fluid- and back-gate of the transistors is stable during this time frame. As it was expected, there is greater variability in the fluid-gate samples due to the manufacturing differences that have been discussed previously, but measurements taken in both gates show highly stable conditions that would facilitate detection of biochemical reactions and molecular binding events that monitor potential changes to identify analytes. Even though the drift is small, for long experiment it can result in signals similar to the ones expected from a 0.25 pH change. Then, for prolonged experiments it will be important to utilize reference sensors to subtract the incidence of drift.

A second robustness analysis can be done by studying the noise power density of the sensors. The BioFET noise spectrum is an important parameter of its operation as it reveals the multiple components contributing to the measured noise. It has been reported previously that an estimate of the spectrum noise can be obtained using Fast Fourier Transforms of a constant drain current measurement [25]. This spectrum reveals the composition of multiple noise components that include electrical, chemical, and drift noise. Fig. 11 shows the noise power density as a function of the frequency of the array. The flicker (1/f) noise and its coefficient (K) are typical for FET sensors, where the slow chemical reactions have the dominating noise component. However, in our platform we also observe harmonic components at higher frequencies. These noise components are related to the multiplexing electronics. Then, our spectrum analysis shows how our sensors have the typical BioFET response with added components due to the switching electronics of the data acquisition system.

4. Performance improvement with dual-gate operation and redundancy techniques

4.1. Dual-gate operation

Sensitivity results presented in section III show the pH response of the devices when operated in a single-gate mode, with a grounded back-gate. However, the DG-BioFETs of our platform enable a dual-gate operation that has been used in the past to obtain beyond Nernst limit sensitivities [22,26–28]. In a constant current dual-gate operation, pH changes that affect the fluid-gate of the sensor must be compensated with the back-side. Then, differences in biasing conditions in each gate and the transconductance of top and bottom devices will allow the amplification of the potential changes. This 'pH amplification' is described by Eq. (3) that defines the dual-gate mode sensitivity amplification factor [29]:

$$\alpha_N = \frac{\mu_1 Cox_1 \left(W/L\right)_1 Vds_1 \left(\psi_{s_1} - 2\varphi_b\right)}{\mu_2 Cox_2 \left(W/L\right)_2 Vds_2 \left(\psi_{s_2} - 2\varphi_b\right)} \quad (3)$$

Where alpha α_N is the dual-gate mode sensitivity amplification, μ is the carrier mobility, *Cox* is the gate capacitance, *Vds* the drain-source voltage, and $\left(\psi_{s_1} - \varphi_b\right)$ represents the biasing condition and level of inversion with ψ_s representing the surface potential and φ_b the energy separation to E_F. Subscripts 1 and 2 refer to the fluid- and back- gate respectively. For dual gate devices μ, W/L, and *Vds* are the same, leaving the dominating amplification factors to the ratio between gate potentials response and dielectric capacitances. In our DG-BioFETs the user can manipulate the biasing of back- and fluid-gate tailoring the α_N sensitivity factor.

Fig. 12 shows the back-gate potential changes of sensors in the array as a function of pH for different fluid biasing conditions to exemplify the DG-BioFETs sensitivity amplification. Dual-gate measurements were performed with a constant V_{FG} and sweeping V_{BG} until obtaining a threshold current of 20 μA. This sampling is quickly performed with our PXI tester and eliminate the effect of external control circuits during the amplification. However, field applications will require constant current circuits to implement the dual-gate operation. Specific biasing conditions, color coded in Fig. 12, modify the measured sensitivity, having greater responses with larger fluid-gate potentials. Fig. 12 also shows how gains in sensitivity are traded for a lower linearity. This effect has been previously reported [19] and will require users to select the operation voltage and amplification factor based on the target application. Applications where a large dynamic range is required will face lower sensitivities but assays where small pH changes are expected and linearity isn't critical can increase the sensitivity by adjusting biasing conditions accordingly.

The sensitivity and fluid-gate biasing relationship is quantified in Fig. 13 that shows the overall sensitivity (slope of the linear regression) as a function of fluid-gate potential. It shows how higher fluid-gate potentials increase the sensitivity but also the recorded noise. Therefore, a resolution analysis is presented in the right axis of Fig. 13 to evaluate the full signal-to-noise performance. The green and red limits in Fig. 13 show the Nernst limit sensitivity and the resolution obtained with the devices in the single-gate operation. Finally, the sensitivity distribution of the devices when biased with

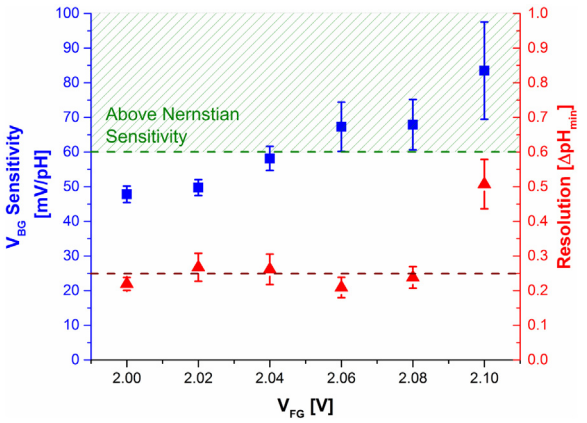

Fig. 13. Sensitivity (blue squares) and resolution (red triangles) as a function of the fluid-gate voltage in dual-gate mode with I_{th} = 20 μA. Error bars represent the standard deviation of all the sensors in the array excluding the 'dummy' diagonal. (For interpretation of the references to colour in this figure legend, the reader is referred to the web version of this article.)

V_{FG} 2.06 V, where we achieved the best resolution, is presented in Fig. 14.

The dual-gate operation allows the user to tailor the sensor's sensitivity. The technique has been studied in multiple devices that have demonstrated very large sensitivity gains, especially when W/L ratios or capacitances are manipulated [22,28]. However, sensitivity gains are frequently accompanied by noise increments that may worsen the resulting resolution. Therefore, using sensitivity amplification schemes requires careful selection of biasing conditions so the signal is maximized while there are acceptable noise increments.

4.2. Filtering based on performance metrics

A key advantage of having multiple equivalent sensors in a single platform is the ability to discard elements based on performance metrics or compression techniques. These methods are common practice for platforms with many sensing elements such as piezo-sensor arrays [30], CMOS imaging systems [31], or gas detection clusters [32]. They have been developed to minimize noise, optimize use of bandwidth, or increase sampling and transfer rates. With over a million different DG-BioFET elements in our array, it is possible to apply these concepts in the biosensing platform taking advantage of the massively multiplexed sensing ability. For BioFETs, the key metric of performance is the sensor's pH resolution. The resolution metric takes into account both sensitivity and noise, resulting in a signal-to-noise ratio metric that accurately reflects the ability of the sensor to detect biochemical events [19]. Using the individual pixel resolution calculations presented in Fig. 8, we filtered the data based on a performance metric of 0.25 pH resolution. Devices with larger resolution than the one selected would have a low sensitivity or high noise which indicate issues with the sensing layer or readout circuitry. Fig. 15(a) shows a binary map of the array with rejected and accepted DG-BioFETs under the 0.25 pH resolution metric that discarded 44.6% of the sensors. The map shows how areas of the array that had poor sensitivity are discarded and evidence a spatial division between accepted and rejected elements, indicating that an important source of performance variation are processing conditions of the sensing membrane. After discarding elements, the overall pH sensitivity is recalculated resulting in a 49.5 mV/pH response that represents a 9.3% increment from the full array measurement. In addition, the overall noise for pH experiments is reduced from 5.4 to 3.37 mV representing a 38% improvement. Results are presented in Fig. 15(b) that shows the increased gross pH sensitivity and lower variations across the accepted devices.

Fig. 15 demonstrates the sensing improvements that can be obtained with a resolution threshold equal to the mean of the distribution. The threshold of 0.25 pH was selected to demonstrate the important improvements that can be achieved by discarding underperforming elements. However, the selected threshold should be based on the target application. For example, applications with lax requirements that only demand detection of large pH changes, such as urea detection [17] or nucleotide incorporation[10], can select a large resolution threshold keeping all the transistors for the measurement. But other more complex applications were very small surface potential changes need to be resolved [4] will require a stricter resolution performance and the elimination of more sensors. Then, similarly to the NAND flash chip quality grades, pre-calibrated DG-BioFET chips can be categorized based on their resolution performance and the number of sensors required for defined applications. The performance-based filtering in the DG-BioFET biosensing platform improves the sensing ability of the overall array, demonstrating the benefit of redundant measurements with a massively multiplexed system, but threshold selection must depend on the target application

4.3. Improving differential referencing with redundant measurements

Differential referencing reduces the impact of common-noise sources, such as drift or temperature fluctuations, by subtracting a reference signal from a measured or test signal. With this technique and under the assumption that both sensors are subject to the same common noise, it is possible to improve the signal-to-noise ratio [33]. Differential referencing can be easily applied in the DG-BioFET platform. For example, some of the sensors in the DG-BioFET platform may act as reference while other "testing" sensors

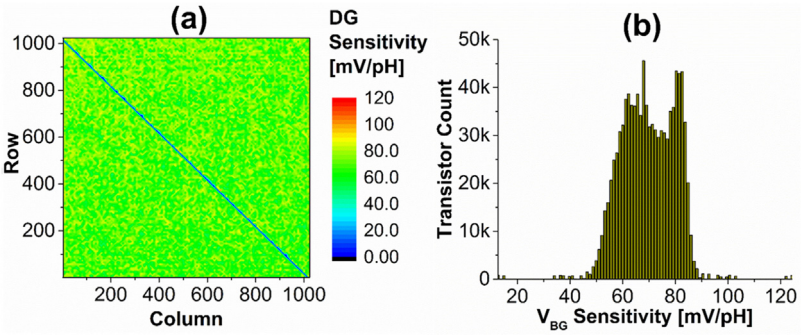

Fig. 14. Individual pixel analysis of dual-gate beyond Nernst limit sensitivity with V_{FG} = 2.06 V and I_{th} = 20 μA. (**a**) Color-coded DG sensitivity. (**b**) Distribution of pH sensitivity in dual-gate operation.

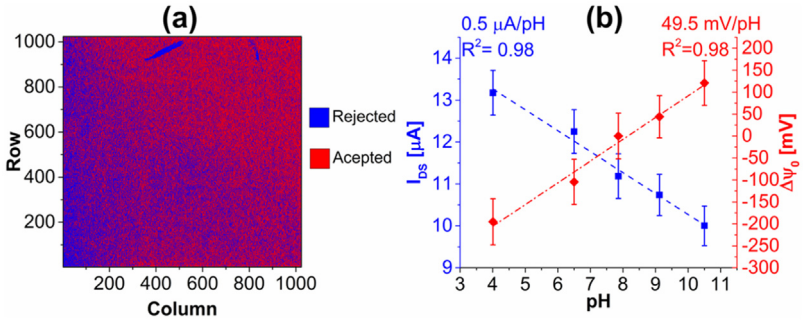

Fig. 15. Selection of pixels based on performance metrics. (**a**) Binary map showing accepted and rejected DG-BioFETs with a metric of resolution at 0.25 pH. (**b**) Drain-current and surface potential sensitivity to pH changes of accepted devices only. Error bars represent standard deviation of sensors in the array. (For interpretation of the references to colour in this figure legend, the reader is referred to the web version of this article.)

are used to measure analytes or reactions. Then, testing and reference signals can be subtracted to eliminate or minimize common noise.

The success of differential referencing, however, relies on low sample to sample variation. A good reference device for differential referencing should have the same response as the testing device. In addition, the reference and testing devices should be exposed to the same experimental conditions with the exemption that the testing device is exposed to the analyte while the reference is only exposed to a negative control. In other words, effective differential referencing requires two identical sensors, subject to the same conditions but having reference sensors monitoring a negative control while the testing sensor monitors the target analyte. Unfortunately, as it has been previously discussed, DG-BioFETs in the platform may have different responses. These differences between sensors are associated with tolerances and defects during the fabrication process that are difficult to overcome. Then, in the DG-BioFET platform using differential referencing may have limited signal-to-noise ratio improvements as reference and testing devices may not have the same response.

To overcome poor uniformity limitations and effectively use differential referencing, redundancy techniques can be used to minimize sample-to-sample variations. With a sampling of rate of less than a millisecond per measurement and over a million devices, the DG-BioFET platform can minimize sample to sample variation by creating groups of reference sensors measuring the same electrolyte, and groups of testing sensors also measuring the same electrolyte. These redundant measurements can be used to reduce sample to sample variation by generating many data points that reveal the true value of the measured variable. Redundancy techniques have been used in the past to eliminate or reduce the effect of outlier events and to improve the accuracy of comparisons between data sets by minimizing variability under the central limit theorem and its relation to the sample size [34]. In fact, the effectiveness of these methods has already been demonstrated in FET sensing platforms that reduce noise by increasing the number of sensors [14].

Fig. 16 presents sample to sample variation as a function of the number of sensors being used for reference and testing of reactions. Fig. 16 shows that the sample to sample variation decreases as more sensors are used to monitor the samples. Having lower variations between samples enable better differential referencing by reducing the influence of sensors with abnormal behaviors. For example, the effect of a sensor with a poor sensitivity decreases when multiple sensors are used to monitor the same reaction. Fig. 16 shows that significant variation decrements are observed up to around 50 sensors but the improvement is small with more sensors. This trend indicates that after a certain number of sensors spatial related effects, such as the variations that have been observed in the current heat maps, would weight in the sample-to-sample variation limiting its reduction. In other words, as the sample of sensors increases, spatial sensitivity differences contribute to the sample-to-sample variations and stagnate improvement. Unfortunately, the sample to sample variation does not follow the $1/\sqrt{\sigma}$ reduction that is expected with normal distributions because external variables, such as differences between sensors in different sections of the array, distort the normality of the distribution.

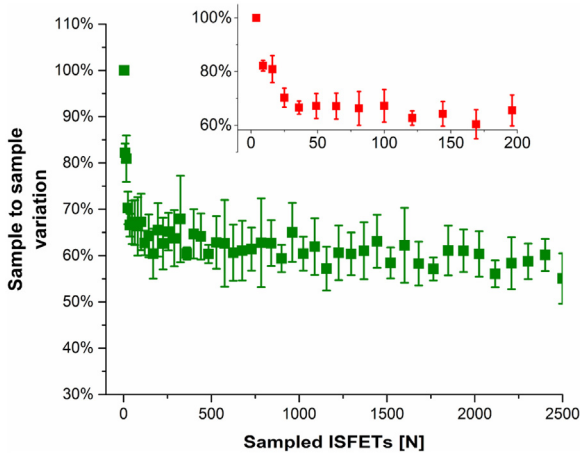

Fig. 16. Spatial redundancy strategies to minimize sample to sample variation as a function of the number of DG-BioFETs used to monitor reactions. The inset zooms in the 0–200 sensors area. Error bars represent the standard deviations between 10 different sample to sample experiments.

Even though the spatial redundancy has a capped improvement, the massive number of devices in our platform is valuable. The chip has been designed to perform parallel reactions and the high density of sensors enables multiplexing and for example, using multiple pairs of reference and testing *groups* within the array to monitor multiple reactions.

Redundancy strategies can be employed to handle measurements in noisy environments by improving differential referencing. This is one of the intrinsic advantages of a massively parallel DG-BioFET platform with integrated circuitry for fast data acquisition. The inherent variability of the fabrication process of BioFETs and the variations of the biochemical events that are investigated with FET biosensors can be managed by using iterative and redundant measurements. The ability to quickly collect large data sets improve accuracy and simplifies quantitative conclusions that describe the detection of entities and differences in the response between target and control samples.

5. Conclusions

In this paper, we present a massively multiplexed dual-gated BioFET sensing platform with over one million devices organized in a 1024×1024 array of $7 \times 7\,mm^2$. The transistors are addressed with an on-chip row and column decoding circuit that quickly obtains drain current measurements for each sensor scanning the full array in around 90s. We presented transfer characteristics of a typical BioFET array, evaluated its pH sensitivity, and estimated the minimum pH change that the sensors can resolve. This characterization revealed distributions of the DG-BioFET sensors performance and spatial variations in the array. In addition, our studies indicate that the sensors have a low drift and a standard 1/f noise spectrum with additional components related to the multiplexor switching. Our unique sensor structure and the large number of devices in our array allowed us to study strategies to improve the sensing performance. The dual-gate operation available in our platform can be used to achieve a sensitivity above the Nernst limit, up to 84 mV/pH. Furthermore, the large number of sensors and high rate of data acquisition enable filtering and redundancy techniques to improve robustness and sensitivity. Depending on the target application and resolution requirements, performance thresholds can be easily applied to discard underperforming sensors and improve the quality of the collected data. Also, spatial redundant measurements reduce variations between groups of sensors, minimize the effect of random events, and facilitate differential referencing. The good pH sensitivity that can be achieved in our platform in conjunction with the versatility that results from the dual-gate operation and the power of a million sensors working in parallel will facilitate the introduction of FET biosensors as the core transduction of sensing elements.

Following Moore's law, the electronic industry has experienced an unprecedented pace of evolution and improvement doubling the capacity of their systems every two years for the last 50 years. BioFET sensors create a pathway to bring that level of innovation and advancement into the diagnostics and biological sensing fields. With the 1024×1024 DG-BioFET platform we have developed a tool that exploits the intrinsic advantages of semiconductor biosensors creating a miniaturized, inexpensive, and massively multiplexed tool for label-free detection of reactions. We have demonstrated the ability of our sensors to detect changes in the electrolyte by monitoring pH. Given the unique characteristics and versatility of our platform with dual-gate operation, redundant measurements, and large sensing area, we foresee multiple applications for our platform. The development of FET-based point-of-care devices [10] can greatly benefit from the dual-gate operation because the biasing manipulation will maximize signal in noisy environments. With the transistors in close proximity to the gate dielectric (i.e. no extended-gate) our sensors can also be used for cell adhesion and metabolisms studies [14]. And finally, the use of the DG-BioFET array for label-free direct molecular detection will allow the interrogation of larger and more complex screening assays [12]. The DG-BioFET array is an inexpensive and high-performing semiconductor biosensor able to improve research and diagnostic tools. The versatility and multiplexing ability of the DG-BioFET array shows the potential benefits of incorporating semiconductor devices in biological applications and open a pathway for new biosensing devices.

Acknowledgments

The authors would like to thank Dr. Andrew Fischer from Abbott Laboratories (Dallas, TX) for useful discussions, USDA ARS for funding support through the Center for Food Safety Engineering (project number 1935–42000-035), and Taiwan Semiconductor Manufacturing Company (TSMC) for providing wafers and technical guidance.

References

[1] B. Veigas, E. Fortunato, P. Baptista, Field effect sensors for nucleic acid detection: recent advances and future perspectives, Sensors 15 (2015) 10380–10398, http://dx.doi.org/10.3390/s150510380.
[2] L. Wang, G.Z. Yang, J. Huang, J. Zhang, L. Yu, Z. Nie, D.R.S. Cumming, A wireless biomedical signal interface system-on-chip for body sensor networks, IEEE Trans. Biomed. Circuits Syst. 4 (2010) 112–117, http://dx.doi.org/10.1109/TBCAS.2009.2038228.
[3] C. Guiducci, F.M. Spiga, Another transistor-based revolution: on-chip qPCR, Nat. Methods 10 (2013) 617–618, http://dx.doi.org/10.1038/nmeth.2525.
[4] B.R. Dorvel, B. Reddy, J. Go, C. Duarte-Guevara, E. Salm, M.A. Alam, R. Bashir, Silicon nanowires with high-k hafnium oxide dielectrics for sensitive detection of small nucleic acid oligomers, ACS Nano 6 (2012) 6150–6164, http://dx.doi.org/10.1021/nn301495k.
[5] M. Kalofonou, C. Toumazou, A low power sub- μW chemical gilbert cell for ISFET differential reaction monitoring, IEEE Trans. Biomed. Circuits Syst. 8 (2014) 565–574, http://dx.doi.org/10.1109/TBCAS.2013.2282894.
[6] N. Nikkhoo, P.G. Gulak, K. Maxwell, Rapid detection of E.Coli bacteria using potassium-sensitive FETs in CMOS, IEEE Biomed. Circuits Syst. Conf. 7 (2012) 168–171, http://dx.doi.org/10.1109/BioCAS.2012.6418470 (2012).
[7] X. Huang, H. Yu, X. Liu, Y. Jiang, M. Yan, D. Wu, A dual-mode large-arrayed CMOS ISFET sensor for accurate and high-throughput pH sensing in biomedical diagnosis, IEEE Trans. Biomed. Eng. 62 (2015), http://dx.doi.org/10.1109/TBME.2015.2419233 (1-1).
[8] J.M. Rothberg, W. Hinz, T.M. Rearick, J. Schultz, W. Mileski, M. Davey, J.H. Leamon, K. Johnson, M.J. Milgrew, M. Edwards, J. Hoon, J.F. Simons, D. Marran, J.W. Myers, J.F. Davidson, A. Branting, J.R. Nobile, B.P. Puc, D. Light, T. a Clark, M. Huber, J.T. Branciforte, I.B. Stoner, S.E. Cawley, M. Lyons, Y. Fu, N. Homer, M. Sedova, X. Miao, B. Reed, J. Sabina, E. Feierstein, M. Schorn, M. Alanjary, E. Dimalanta, D. Dressman, R. Kasinskas, T. Sokolsky, J.A. Fidanza, E. Namsaraev, K.J. McKernan, A. Williams, G.T. Roth, J. Bustillo, An integrated semiconductor device enabling non-optical genome sequencing, Nature 475 (2011) 348–352, http://dx.doi.org/10.1038/nature10242.
[9] B. Merriman, I.T. R&D Team, J.M. Rothberg, Progress in Ion Torrent semiconductor chip based sequencing, Electrophoresis 33 (2012) 3397–3417, http://dx.doi.org/10.1002/elps.201200424.
[10] C. Toumazou, L.M. Shepherd, S.C. Reed, G.I. Chen, A. Patel, D.M. Garner, C.-J. Wang, C.-P. Ou, K. Amin-Desai, P. Athanasiou, H. Bai, I.M.Q. Brizido, B. Caldwell, D. Coomber-Alford, P. Georgiou, K.S. Jordan, J.C. Joyce, M. La Mura, D. Morley, S. Sathyavruthan, S. Temelso, R.E. Thomas, L. Zhang, Simultaneous DNA amplification and detection using a pH-sensing semiconductor system, Nat. Methods 10 (2013) 641–646, http://dx.doi.org/10.1038/nmeth.2520.
[11] M.R. Hartman, R.C.H. Ruiz, S. Hamada, C. Xu, K.G. Yancey, Y. Yu, W. Han, D. Luo, Point-of-care nucleic acid detection using nanotechnology, Nanoscale 5 (2013) 10141–10154, http://dx.doi.org/10.1039/c3nr04015a.
[12] P. Livi, M. Kwiat, A. Shadmani, A. Pevzner, G. Navarra, J. Rothe, A. Stettler, Y. Chen, F. Patolsky, A. Hierlemann, Monolithic integration of a silicon nanowire field-effect transistors array on a complementary metal-oxide semiconductor chip for biochemical sensor applications, Anal. Chem. 87 (2015) 9982–9990, http://dx.doi.org/10.1021/acs.analchem.5b02604.
[13] M. Crescentini, M. Bennati, M. Carminati, M. Tartagni, Noise limits of CMOS current interfaces for biosensors: a review, IEEE Trans. Biomed. Circuits Syst. 8 (2014) 278–292, http://dx.doi.org/10.1109/TBCAS.2013.2262998.
[14] B.C. Cheah, A.I. Macdonald, C. Martin, A.J. Streklas, G. Campbell, M.A. Al-rawhani, B. Nemeth, J.P. Grant, M.P. Barrett, D.R.S. Cumming, An integrated circuit for chip-based analysis of enzyme kinetics and metabolite quantification, IEEE Trans. Biomed. Circuits Syst. 10 (2016) 721–730.
[15] B. Nemeth, M.S. Piechocinski, D.R.S. Cumming, High-resolution real-time ion-camera system using a CMOS-based chemical sensor array for proton imaging, Sens. Actuators B Chem. 171–172 (2012) 747–752, http://dx.doi.org/10.1016/j.snb.2012.05.066.
[16] G. Nabovati, E. Ghafar-Zadeh, M. Sawan, A 64 pixel ISFET-based biosensor for extracellular pH gradient monitoring, IEEE Circuits Syst. (ISCAS) 2015 (2015) 1762–1765 http://ieeexplore.ieee.org/xpls/icp.jsp?arnumber=7168995.
[17] T. Chen, C. Wen, J. Huang, Y. Peng, S. Liu, S. Su, L. Cheng, H. Lai, F. Lai, C. Cheng, C. Yang, J. Yang, Y. Hsieh, E. Salm, B. Reddy, F. Tsui, R. Bashir, M. Chen, A semiconductor bio-electrical platform with addressable thermal control circuits for accelerated bioassay development, Electron Devices Meet (2014) 390–393 http://ieeexplore.ieee.org/stamp/stamp.jsp?arnumber=7047058.
[18] S. Ingebrandt, Bioelectronics: sensing beyond the limit, Nat. Nanotechnol. 10 (2015) 734–735, http://dx.doi.org/10.1038/nnano.2015.199.
[19] C. Duarte-Guevara, F.-L. Lai, C.-W. Cheng, B. Reddy, E. Salm, V. Swaminathan, Y.-K. Tsui, H.C. Tuan, A. Kalnitsky, Y.-S. Liu, R. Bashir, Enhanced biosensing resolution with foundry fabricated individually addressable dual-gated ISFETs, Anal. Chem. 86 (2014) 8359–8367, http://dx.doi.org/10.1021/ac501912x.
[20] E. Salm, Y. Zhong, B. Reddy Jr, C. Duarte-Guevara, V. Swaminathan, Y.-S. Liu, R. Bashir, Electrical detection of nucleic acid amplification using an on-chip quasi-reference electrode and a PVC REFET, Anal. Chem. 86 (2014) 6968–6975, http://dx.doi.org/10.1021/ac500897t ((accessed September 7, 2014).

[21] C. Duarte-Guevara, V.V. Swaminathan, M. Burgess, B. Reddy, E. Salm, Y.-S. Liu, J. Rodriguez-Lopez, R. Bashir, On-chip metal/polypyrrole quasi-reference electrodes for robust ISFET operation, Analyst 140 (2015) 3630–3641, http://dx.doi.org/10.1039/C5AN00085H.
[22] J. Go, P. Nair, B. Reddy Jr, B. Dorvel, Coupled heterogeneous nanowire—nanoplate planar transistor sensors for giant (>10 V/pH) Nernst response, ACS Nano 6 (2012) 5972–5979, http://dx.doi.org/10.1021/nn300874w (accessed October 30, 2012).
[23] J.L. Chiang, S.S. Jan, J.C. Chou, Y.C. Chen, Study on the temperature effect, hysteresis and drift of pH-ISFET devices based on amorphous tungsten oxide, Sens. Actuators B Chem. 76 (2001) 624–628, http://dx.doi.org/10.1016/S0925-4005(01)00657-8.
[24] D.-H. Kwon, B.-W. Cho, C.-S. Kim, B.-K. Sohn, Effects of heat treatment on Ta2O5 sensing membrane for low drift and high sensitivity pH-ISFET, Sens. Actuators B Chem. 34 (1996) 441–445, http://dx.doi.org/10.1016/S0925-4005(96)01938-7.
[25] Y. Hu, P. Georgiou, A robust ISFET pH-measuring front-end for chemical reaction monitoring, IEEE Trans. Biomed. Circuits Syst. 8 (2014) 177–185, http://dx.doi.org/10.1109/TBCAS.2014.2313512.
[26] H.J. Jang, W.J. Cho, Fabrication of high-performance fully depleted silicon-on-insulator based dual-gate ion-sensitive field-effect transistor beyond the Nernstian limit, Appl. Phys. Lett. 100 (2012), http://dx.doi.org/10.1063/1.3685497.
[27] M. Spijkman, E.C.P. Smits, J.F.M. Cillessen, F. Biscarini, P.W.M. Blom, D.M. de Leeuw, Beyond the Nernst-limit with dual-gate ZnO ion-sensitive field-effect transistors, Appl. Phys. Lett. 98 (43502) (2011), http://dx.doi.org/10.1063/1.3546169.
[28] O. Knopfmacher, A. Tarasov, W. Fu, M. Wipf, B. Niesen, M. Calame, C. Schönenberger, Nernst limit in dual-gated Si-nanowire FET sensors, Nano Lett. 10 (2010) 2268–2274, http://dx.doi.org/10.1021/nl100892y.
[29] J. Go, P.R. Nair, M.A. Alam, Theory of signal and noise in double-gated nanoscale electronic pH sensors Theory of signal and noise in double-gated nanoscale electronic p H sensors, J. Appl. Phys. 34516 (2012) 1–10, http://dx.doi.org/10.1063/1.4737604.
[30] P. De Boe, J.-C. Golinval, Principal component analysis of a piezosensor array for damage localization, Struct. Heal. Monit. 2 (2003) 137–144, http://dx.doi.org/10.1177/1475921703002002005.
[31] M. Zhang, Compressive acquisition CMOS image sensor: from algorithm to hardware implementation, IEEE Trans. Very Large Scale Integr. 18 (171) (2010), http://dx.doi.org/10.1109/TVLSI.2008.2011489.
[32] M. Ni, J.R. Stetter, W.J. Buttner, Orthogonal gas sensor arrays with intelligent algorithms for early warning of electrical fires, Sens. Actuators B Chem. 130 (2008) 889–899, http://dx.doi.org/10.1016/j.snb.2007.10.070.
[33] K.J. Paralikar, C.R. Rao, R.S. Clement, New approaches to eliminating common-noise artifacts in recordings from intracortical microelectrode arrays: inter-electrode correlation and virtual referencing, J. Neurosci. Methods 181 (2009) 27–35, http://dx.doi.org/10.1016/j.jneumeth.2009.04.014.
[34] W.X.Y. Li, R.C.C. Cheung, R.H.M. Chan, D. Song, T.W. Berger, Real-time prediction of neuronal population spiking activity using FPGA, IEEE Trans. Biomed. Circuits Syst. 7 (2013) 489–498, http://dx.doi.org/10.1109/TBCAS.2012.2228261.

Biographies

Carlos Duarte-Guevara Completed his Ph.D. in electrical and computer engineering at the University of Illinois in Urbana Champaign in 2016. He is currently a technical specialist at Finnegan, Henderson, Farabow, Garrett & Dunner, LLP.

Vikhram Swaminathan Completed his Ph.D. in mechanical engineering at the University of Illinois in Urbana Champaign in 2015. He currently works at Lam Research Corporation.

Bobby Reddy, Jr Completed his Ph.D. in electrical and computer engineering at the University of Illinois in Urbana Champaign in 2016. Currently works at Prenosis inc.

Chin-Hua Wen Completed his M.Sc. in National Tsing Hua University. Currently works for Taiwan Semiconductor Manufacturing Company.

Yu-Jie Huang Completed his Ph.D. at National Taiwan University. Currently works for Taiwan Semiconductor Manufacturing Company.

Jui-Cheng Huang Currently works for Taiwan Semiconductor Manufacturing Company.

Yi-Shao Liu Completed his Ph.D. in electrical and computer engineering at Purdue University. He is current a Delta Electronics.

Rashid Bashir Joined Purdue University in Oct. 1998 as an Assistant Professor and was later promoted to Professor of Electrical and Computer Engineering and a Courtesy Professor of Biomedical Engineering and Mechanical Engineering. Since Oct. 2007, he joined the University of Illinois at Urbana-Champaign and was the Abel Bliss Professor of Engineering, and Professor of Electrical and Computer Engineering & Bioengineering. He was the Director of the Micro and Nanotechnology Laboratory (mntl.illinois.edu), a campus-wide clean room facility from Oct 2007 to Aug 2013 and the Co-Director of the campus-wide Center for Nanoscale Science and Technology (www.cnst.illinois.edu), a collaboratory aimed at facilitating center grants and large initiatives around campus in the area of nanotechnology. In Oct 2016, he was named the Grainger Distinguished Chair in Engineering. Since Aug 2013, he has been the head of the Bioengineering Department. From Jan 2017, he will also be the Interim Vice Dean of the new Carle-Illinois 'Engineering Based' College of Medicine at UIUC.